World Conference on Timber Engineering Oslo 2023

MECHANICAL BEHAVIOUR OF COLUMN BASES FOR CLT ROCKING FRAMES

Akira Masuda[1], Chisato Inutsuka[2], Kazuhiro Matsuda[3]

ABSTRACT: Although Cross Laminated Timber (CLT) mid-to-high-scale buildings have been realised worldwide, the technology for controlling damage in these buildings, which could minimise damage and facilitate continued use of buildings after a significant earthquake, is still in the developmental stage. In this study, a static horizontal loading experiment was conducted on CLT wall columns with origin return characteristics by introducing prestress, and the mechanical behaviour of the CLT wall columns was investigated. We determined the difference in the origin return characteristics and damage of wall columns when the prestress introduced to the wall columns and the diameter of the PC bar were varied. We also propose a method to evaluate the relationship between the bending moment and rotation angle of the column base. The evaluation method applies calculations that are commonly used for joints in large wooden buildings. In this case, it was necessary to evaluate the uplift of the column base in advance, and we created a spring model to evaluate the uplift. Although this evaluation method has some limitations, it is believed that the experimental results can be accurately replicated.

KEYWORDS: CLT, Rocking Wall-Column, Prestress, Embedding Stiffness, Anchorage Plate

1 INTRODUCTION

1.1 BACKGROUND

Due to the social imperative of sustainable and healthy forestry development and environmental CO_2 reduction, there is increasing demand for mid-to-high-rise wooden buildings, leading to the proliferation of Cross Laminated Timber (CLT). In general, CLT buildings use CLT panels as walls and floors (e.g. in Japan, CLT panel buildings [1]). However, because the restoring force characteristics exhibit slip behaviour [2, 3], it may be difficult to maintain the function after a large earthquake. Thus, developing damage control technology for CLT buildings to minimise damage and enable continued use after large earthquakes is crucial.

Matsuda et al. [4] conducted an experiment on a passively controlled CLT structure, utilising both a rocking wall column and a damper, resulting in a structure with reduced residual deformation and high energy absorption performance. While the behaviour of the frame was analysed, the behaviour of the wall column was not comprehensively identified.

Pei et al. [5], Sarti et al. [6], and Iqbal et al. [7] conducted research on damage control structures for mid-to high-scale wooden buildings. Pei et al. introduced prestressing by placing PC bar at the centre of the CLT wall column. This wall column was deformed by uplift while rotating the column base. Because the slip is reduced by prestress, the wall column is a structural system with high-origin return characteristics.

Isoda et al. [8] examined the implementation of Japanese specifications by referring to CLT rocking columns overseas. Harada et al. [9], Komoriya et al. [10], and Tanaka et al. [11] proposed CLT shear walls with a PC bar inserted at each edge of the wall column. In addition, Nagashima et al. [12] conducted an experiment on a laminated wood wall column in which prestress was introduced with a PC bar and proposed an evaluation method with high reproducibility in the elastic region.

1.2 PURPOSE AND STRUCTURE

In this study, a static horizontal loading experiment was conducted on CLT wall columns with origin return characteristics by introducing prestress to investigate the mechanical behaviour of the CLT wall column. We proposed a method for evaluating the relationship between the bending moment and rotation angle of the column base.

Figure 1 shows an image of the mid-to high-scale wooden buildings proposed in this study. By introducing a passively controlled CLT structure into a part of a general CLT building, such as a CLT panel building [1], we realise a mid-to-high-scale wooden building with excellent performance maintenance after an earthquake. The PC bar, which introduces prestress, is anchored to the column capital and the column base of the passively controlled frame with an anchorage plate. Steel dowels were used as the shear resistance for the column base. By creating steel dowel details that do not resist pulling

[1] Akira Masuda, Grad. Student, Meijo University of Sci. and Eng., Mr. Eng., Japan, 223443503@ccalumni.meijo-u.ac.jp
[2] Chisato Inutsuka, Grad. Student, Meijo University of Sci. and Eng., Japan, 213435002 @ccalumni.meijo-u.ac.jp
[3] Kazuhiro Matsuda, Associate Prof., Dept. of Architecture, Meijo University, Dr. Eng., japan, matsuda@meijo-u.ac.jp

https://doi.org/10.52202/069179-0044

out, that details actively causes rotation and rocking of the column base. Steel dowels were installed at the column-beam joint, and a tensile bolt was installed at the centre of the beam to actively cause rotational deformation at the column-beam joint of the passively controlled frame. However, a damper is installed in the passively controlled CLT frame because the prestressed wall column alone does not have sufficient seismic energy-absorbing performance. In addition, because the effect of creep cannot be neglected when the stress level increases, we assume that the detail of the passively controlled frame minimises the burden of long-term axial force on the wall columns. Section 2 describes the outline and results of the static experiment. Chapter 3 proposes an evaluation procedure for the relationship between the bending moment and the rotation angle of the column base.

2 STATIC EXPERIMENT WITH CLT ROCKING WALL COLUMNS

2.1 EXPERIMENT OUTLINE

Figure 2 shows the shapes of the specimens. The five specimens were RW0, RW30, RW50, RW30φS, and RW30φL, and CLT rocking wall columns with a width of 1,000 mm and a height of 2,970 mm. The CLT was composed of five layers and six plies of cedar (the thickness of one lamina was 25 mm), the strength grade was S60, and the cross-sectional dimensions were 150 mm × 1000 mm. A 30 mm × 30 mm through-hole was made at the centre of the cross-section of the CLT to insert the PC bar. A groove of 15 mm × 30 mm was made in the centre of three layers and three plies of CLT, and the through-hole was made by secondarily adhering the two CLTs with the grooves facing each other. The PC bar was anchored by the anchorage plate provided on the column capital and jig for fixing. The anchorage plate on the column was a 500 mm × 150 mm × 32 mm SS400 steel plate with a φ30 mm hole in the centre. The anchorage plate of the fixing jig was made of SS400 with a thickness of 60 mm, which is sufficiently stronger than that of the column capital. Two φ50 steel dowels were provided on the column base as shear resistance.

Table 1 lists the prestress applied to each specimen and the diameter of the PC-bar used for each specimen. The introduced prestresses were 0%, 30%, and 50% of the long-term allowable compressive strength, corresponding to the numbers in the names of the specimens. The long-term allowable compressive strength is the standard strength [1] multiplied by 1.1/3, and the cross-sectional area. The PC bars used were B2-type (manufactured by Neturen), with diameters of φ17, φ23, and φ32. ϕS in the name of the specimen corresponds to φ17, φL to φ32, and no dose to φ23.

Figure 3 shows the setup of the experimental specimen. The steel dowels and anchorage plate of the foundation were firmly fixed to the fixing jig using bolts. After the two points of the column capital were constrained out of the plane with the pantograph, a 200kN oil jack was connected at a height of 2,400 mm from the column base, and positive and negative alternating loads were applied. The positive force direction is shown on the right in

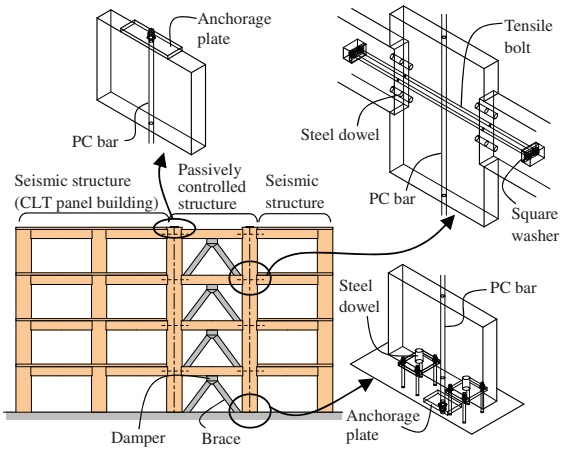

***Figure 1**: The building proposed in this study*

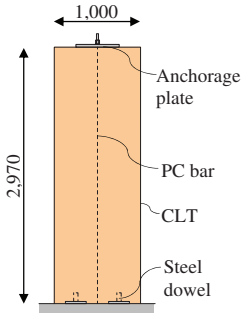

***Table 1**: Specimen list*

Specimen list		
Name	Prestress	PC-bar size
RW0	0%	φ23
RW30	30%	φ23
RW50	50%	φ23
RW30φS	30%	φ17
RW30φL	30%	φ32
Member parameters		
CLT	5 layers 6 plies of cedar	
PC bar	B2-type	
Anchorage plate	SS400 (500*150*32)	
Steel dowel	SS400 (φ50)	

***Figure 2**: Specimens*

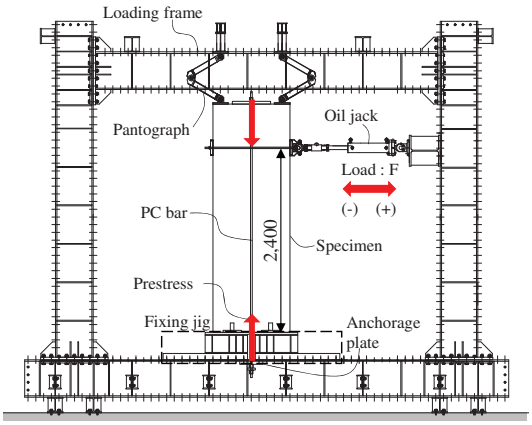

***Figure 3**: Setup*

Figure 3. As for the loading schedule, positive and negative deformations up to 1/450, 1/300, 1/200(1), 1/150, 1/100(1), 1/200(2), 1/75, 1/50, 1/100(2), 1/ 30 and 1/20 rad were repeated three times, and then pulled off in the positive direction. In addition, because the anchorage plate was significantly deformed just before 1/20 rad, RW-30φL was pulled without applying 1/20 rad.

Figure 4 shows the measurement items. The absolute horizontal displacement of the column capital was measured using a wire displacement meter (DP-500G, manufactured by Tokyo Sokki), and the absolute

https://doi.org/10.52202/069179-0044

horizontal displacement of the column base was measured using a contact-type displacement meter (CDP25, Tokyo Sokki). The storey deformation angle θ was obtained by dividing the displacement difference between the column capital and column base by the height of the loaded point. The load was measured using a 200kN load cell attached to the oil jack. Displacement gauges $u_{c\,1}$ and $u_{c\,2}$ were installed on the column base, and the rotation θ_{cb}, uplift u_{cb}, embedded width $x_{n\,cb}$, and bending moment M_{cb} were calculated using Eqs. (1 ~ 4). These equations assume that the embedded triangle and the axial force of the PC bar are balanced. The tensile force acting on the PC bar was measured using a 1000 kN load cell.

2.2 RESULT OF THE EXPERIMENT

Figure 5 shows the relationship between the bending moment of the column base M_{cb} and rotation angle of the column base θ_c. All specimens showed an origin return history and had a high initial stiffness until the bending moment required to release the initial tension was applied. Subsequently, the stiffness decreases as the deformation increases. In (a) RW0, (b) RW30, and (c) RW50, the edge of the column base was damaged, as shown in Figure 6. No CLT damage was observed in (d)RW30φS. (e) RW30φL caused severe damage to the column capital.

(a) RW0 showed no decrease in stress at θ= 1/100 rad (2), indicating that θ= 1/100 rad (1) and θ= 1/100 rad (2) have almost the same history. Therefore, the rocking wall column can be expected to maintain its performance after a severe earthquake. RW0 behaved almost linearly up to 1/50 rad, after which the original return characteristics gradually disappeared.

(b) RW30 showed no decrease in stress at θ= 1/100 rad (2), indicating that θ= 1/100 rad (1) and θ= 1/100 rad (2) had almost the same history. In addition, before θ = 1/30 rad, no significant decrease in yield strength was observed. After experiencing 1/20 rad, the initial stiffness part was lost, and after experiencing maximum deformation, the original return characteristics were also lost. The bending moment required to release the initial tension decreased owing to the decrease in the initial tension of the PC-bar, as shown in Section 2.3.

Considering the initial stiffness in the order of RW-0, RW-30, and RW-50, it can be confirmed that the stiffness increased. In addition, RW50 showed almost the same history at θ= 1/200 rad (2) and θ= 1/200 rad (1), but θ= 1/100 rad (2) is slightly lower than θ= 1/100 rad (1). As

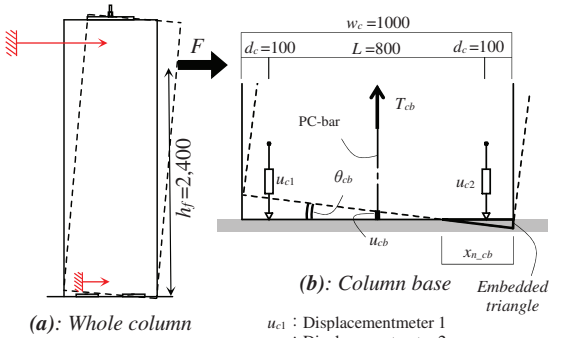

$\theta_{cb} = (u_{c1} - u_{c2})/L$ (1)

$u_{cb} = (u_{c1} + u_{c2})/2$ (2)

$x_{n\_cb} = d_c - u_{c2}/\theta_{cb}$ (3)

$M_{cb} = F * h_f$ (4)

u_{c1} : Displacementmeter 1
u_{c2} : Displacementmeter 2
θ_{cb} : Rotation angle of column base
L : Distance between displacement meters
x_{n_cb} : Embedded width
d_c : Distance from Displacementmeter to wall-column edge
u_{cb} : Uplift of column base at center
T_{cb} : Tensile force of PC-bar
w_c : Wall width
M_{cb} : Bending moment of column base

***Figure 4**: Measurement items*

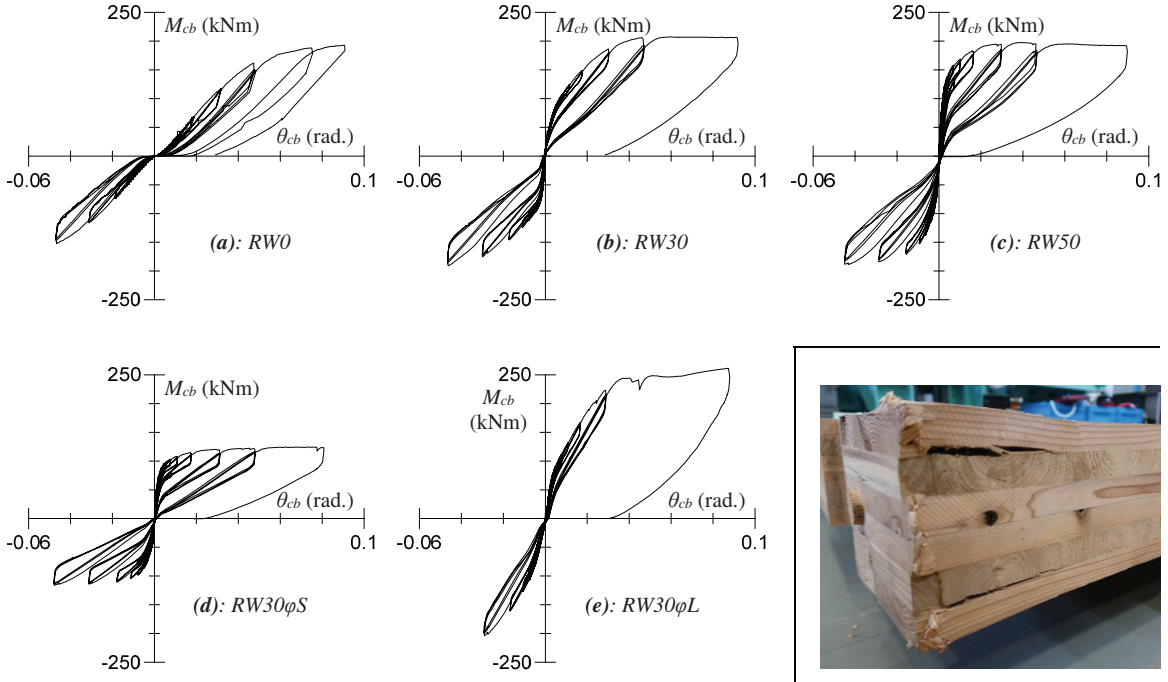

***Figure 5**: Relationship between M_{cb} and θ_{cb}*

***Figure 6**: Destruction property of column base*

https://doi.org/10.52202/069179-0044

the initial tension increased, the initial stiffness increased; however, the CLT was damaged more quickly than RW30. (d) RW30φS of θ=1/100rad(2) is slightly lower than θ=1/100rad(1). After experiencing 1/30 rad, the initial stiffness part was lost, and after experiencing the maximum deformation, the origin return characteristic was also lost.

Observing the order of RW-30φS, RW-30, and RW-30φL, the range in which the initial stiffness is lost decreases. (e) RW-30φL showed no decrease in stress at θ = 1/100 rad(2), indicating that θ = 1/100 rad(1) and θ = 1/100 rad(2) had almost the same history. In addition, before θ = 1/30 rad, no significant decrease in stress was observed, and after experiencing maximum deformation, the original return characteristic was lost.

Figure 7 shows the relationship between the PC-bar tension T_{cb} and uplift of the base column u_{cb}.

RW0 exhibited linear hysteresis, except for the last pull-off, and the maximum yield strength was 389 kN.

RW30 exhibited a maximum yield strength of 419 kN. The hysteresis was linear up to θ=1/50 rad, and the initial stiffness was slightly lower than that of RW0. Subsequently, a decrease in the initial tension was observed when u_{cb} = 0. This decrease in tension is slight at θ = 1/100 rad.(2) and became significant at θ = 1/30 rad.

RW50 had a maximum yield strength of 410 kN. The hysteresis was linear up to θ=1/75 rad, and the initial stiffness was slightly lower than that of RW30. Subsequently, a decrease in the initial tension was observed when u_{cb} = 0.

RW30φS had a maximum yield strength of 230 kN. The hysteresis was linear up to θ=1/150 rad, and the initial stiffness was slightly lower than that of RW30. Subsequently, a decrease in the initial tension was observed when u_{cb} = 0.

RW30φL had a maximum yield strength of 601 kN. The hysteresis was linear up to θ=1/50 rad, and the initial stiffness was slightly higher than that of RW30. Subsequently, a decrease in the initial tension was observed when u_{cb} = 0. Figure 8 shows the anchorage plate of the RW30φL. Just before 1/20 rad, the anchorage plate began to embed into the column capital of CLT while undergoing a large bending deformation, as shown in Figure 8.

Figure 9 shows the changes in the ratio θ_{cb}/θ of the column base rotation angle θ_{cb} and the story deformation angle θ. The vertical axis is θ_{cb}/θ and the horizontal axis is θ. (a) RW0, RW 30, and RW 50 with different prestresses and (b) RW30φS, RW30, and RW30φL with different PC-bar diameters.

RW0 always exhibited a value close to 100%. Because no prestress is introduced in RW0, it is thought that the column base joint behaves closer to a pin joint. The ratio of RW30 was lower at a small deformation than that of RW0 and gradually increased as the deformation increased. Because RW30 has a prestress introduced, it is considered that the ratio of bending deformation and shear deformation of CLT increased, and the behaviour became closer to that of a rigid joint. The ratio of RW50 was lower at a small deformation than that of RW30 and gradually increased as the deformation increased. Because RW50 introduced more prestress than RW30, it is thought that the rate of bending deformation and shear deformation of the CLT increased further. Figure 9(b) shows that there was no significant difference between RW30φS, RW30, and RW30φL.

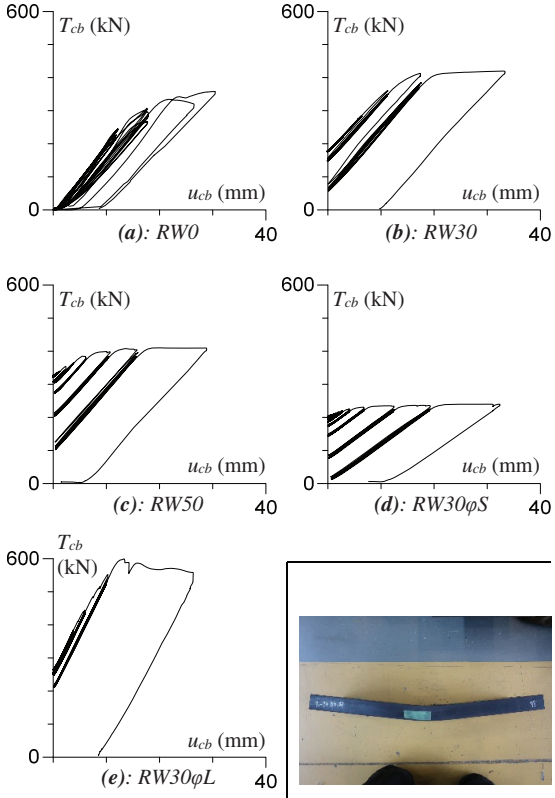

***Figure 7**: Relationship between T_{cb} and u_{cb}*

***Figure 8**: Destruction property of Anchorage plate*

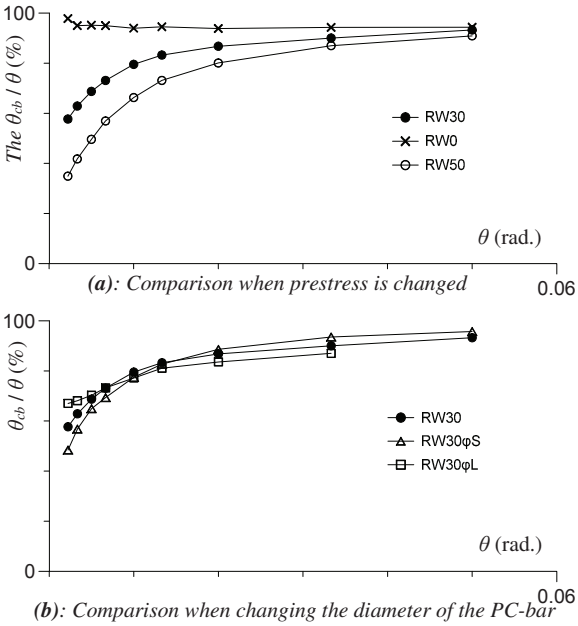

***Figure 9**: Transition in the ratio of θ_{cb} to θ*

https://doi.org/10.52202/069179-0044

3 THEORETICAL EVALUATION METHOD

Figure 10 shows an image of the rotation angle of the column base of the CLT wall column, and Eq. (5) and (6) are the evaluation representing the evaluation methods proposed in [13]. The CLT has a very high in-plane stiffness, and the performance of the column base is directly linked to the performance of the entire CLT wall column. Various parameters, such as M_{cb}, θ_{cb}, and x_{n_cb} must be obtained to evaluate the deformation and stress of the column base. Their parameters are obtained by solving the simultaneous equations of the two equations, the equation of compressive force C_{cb}, Eq. (5), and the equations of compatibility for the embedded triangular, Eq. (6). Their simultaneous equations are solved for θ_{cb} and x_{n_cb} based on the following two points: (i) It is assumed that T_{cb}, tension, and C_{cb}, the compressive force of the embedded triangle, are balanced, (ii) k_g is the slope of the envelope of the CLT-embedded experiment described in Section 3.1. In this case, u_{cb} must be requested in advance.

A mechanical model of u_{cb} is shown in Figure 11. The mechanical model was a spring model with a series combination of K_t: axial stiffness of the PC bar, K_p: embedded stiffness of the anchorage plate, and K_w: compressive stiffness of the CLT middle zone. Here, K_t was created as a skeleton curve with reference to the mill sheet value of the PC-bar. K_p is the envelope of the embedding anchorage plate experiment described in section 3.2. K_w is the envelope of the CLT partial compression experiment described in section 3.3. The skeletal curve of K_t is shown in Table 2 with reference to the mill sheet.

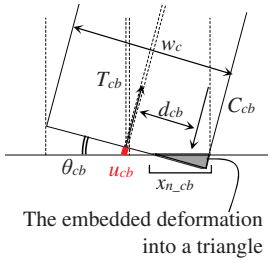

$$T_{cb} = C_{cb} = \frac{1}{2} k_g \theta_{cb} x_{n\_cb}^2 b \quad (5)$$

$$x_{n\_cb} = w_c / 2 - u_{cb} / \theta_{cb} \quad (6)$$

C_{cb} : Compressive force
k_g : Embedding stiffness of column base
b : Wall thickness
d_{cb} : Interval from the point where T_{cb} is applied to the point where C_{cb} is applied

***Figure 10**: Deformation of column base*

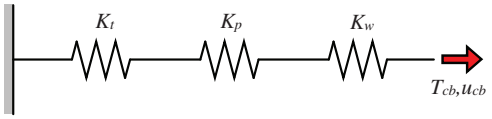

K_t : Axial stiffness of the PC-bar
K_p : Embedded stiffness of the anchorage plate
K_w : Compression stiffness of middle zone in CLT

***Figure 11**: u_{cb} spring model*

***Table 2**: Material characteristic of PC-bar*

σ_t [N/mm^2]	ε_t [%]
1042	0.51
1136	14

3.1 THE EMBEDDED CLT EXPERIMENT

Figure 12 shows the specimens of the CLT-embedded experiment, which were created by cutting out the less damaged parts of the specimens in the static horizontal loading experiment. The number of specimens is 4. The force position was at the edge of the specimens, and a steel plate (19 × 100 × 260 mm) was used to load vertically downwards. The measurement parameters were the load T_g and absolute vertical displacement δ_g of the steel plate. Figure 13 shows the relationship between the stress σ_g and embedding displacement δ_g. The σ_g–δ_g relations of the four specimens were averaged, and the embedded stiffness was a straight line approximated by the least-squares method between 10% and 40% of the maximum stress. The yield stress was considered as the average value of the highest stress point.

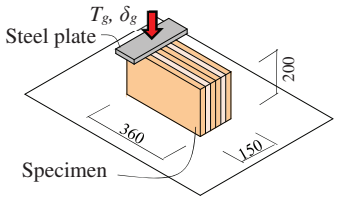

***Figure 12**: The CLT embedded experiment*

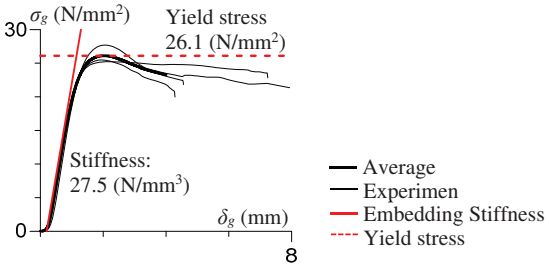

***Figure 13**: The relationships between σ_g and δ_g*

3.2 THE EMBEDDING ANCHORAGE PLATE EXPERIMENT

Figure 14 shows the setup of the embedded anchorage plate. The specimens were created by cutting out the less damaged parts from the wall column specimens. The number of specimens is 3. The anchorage plate was loaded by pulling the PC bar with the centre-hole jack. The measurement items are the tension of the PC-bar, T_p, and the embedding displacement of the anchorage plate, x_p. Figure 15 shows the relationship between T_p and x_p. Note that x_w is the deformation up to 28 mm from the top surface of the CLT.

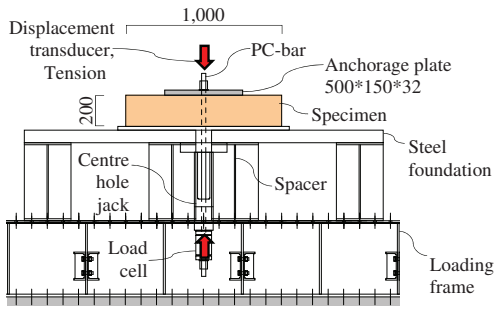

***Figure 14**: The experiment of the embedding anchorage plate*

https://doi.org/10.52202/069179-0044

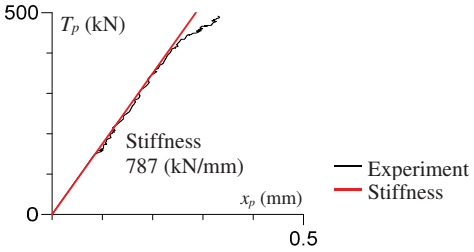

***Figure 15**: The relationships between T_p and x_p*

3.3 THE CLT PARTIAL COMPRESSION EXPERIMENT

Figure 16 shows the setup of the CLT partial compression experiment. The CLT used was different from that used in the static horizontal loading experiment. To understand the difference in the material properties from the CLT of the static horizontal loading experiment, a separate CLT material experiment was conducted. The number of specimens used was one. Assuming a rocked wall column, a load was applied to the centre of the column capital and the edge of the column base. The specimen was loaded with a 500kN oil jack and was placed so that the three points were on the same straight line: (i) the centre of the jack, (ii) the centre of the load-applying surface on the column capital, and (iii) the centre of the load-applying surface on the column base (hereafter referred to as "the load line"). Fifty-ton pins were installed on the column capital and base of the CLT wall column. The 50-ton pin on the column base side was fixed to the loading frame and that on the column capital side was connected to the oil jack. The right end of the oil jack was fixed to the loading frame, and the lower left end of the oil jack was connected to a linear rail that moved only in the direction of the load line. The measurement items were T_w, the load of the jack, and, x_w, the compressive deformation of the CLT on the load line. Note that x_w does not include deformations within 28 mm above and below the CLT. Figure 17 shows the relationship between T_w and x_w.

3.4 METHOD OUTLINE

T_0 evaluate the column base, it is necessary to calculate u_{cb} in advance. The mechanical model of u_{cb} is a spring model with a series combination of K_t, K_p, and K_w. The tension T_{cb} applied to the spring model is the sum of T_0, the initial tension, and dT, the tension change amount after the introduction of the initial tension, as shown in Eq. (7). dT was varied at 0.1 kN increments. The u_{cb} is the sum of dx_t, dx_p, and dx_w; each deformation change amount of the element after the introduction of T_0 as shown in Eq. (8). dx_t, dx_p, and dx_w are the differences between x_t, x_p, x_w, each deformation of the element at T_{cb} and x_{t0}, x_{p0}, x_{w0}, each deformation of the element when T_0 is introduced, as shown in Eqs. (9–11). x_t: The deformation of the PC bar at T_{cb} was calculated using Eq. (12), and x_{t0}, the deformation of the PC-bar when T_0 was introduced and calculated using Eq. (13). x_p, the embedding deformation of the anchorage plate was used as the result of the embedding anchorage plate experiments obtained in Section 3.2. x_w, compression deformation of the CLT middle zone was used as the result of the wall column

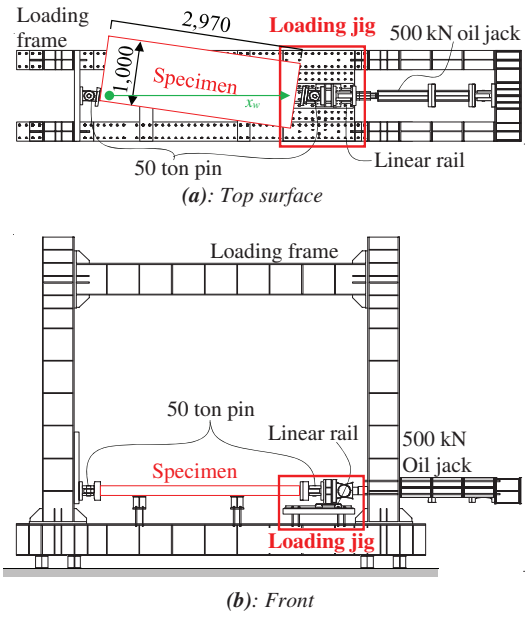

***Figure 16**: The experiment of the CLT partially compressed*

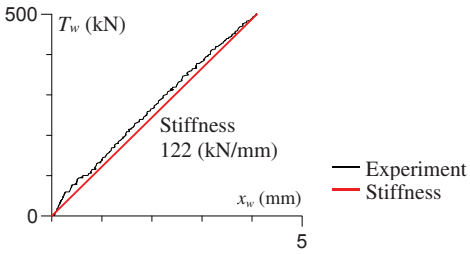

***Figure 17**: The relationships between T_w and x_w*

$$T_{cb} = T_0 + dT \quad (7)$$

$$u_{cb} = dx_t + dx_p + dx_w - x_{g0} \quad (8)$$

$$dx_t = x_t - x_{t0} \quad (9)$$

$$dx_p = x_p - x_{p0} \quad (10)$$

$$dx_w = x_w - x_{w0} \quad (11)$$

$$x_t = T_{cb} / K_t \quad (12)$$

$$x_{t0} = T_0 / K_t \quad (13)$$

$$K_t = A_t E_t / h_t \quad (14)$$

T_0: Initial tension
dT: Tension increase after the introduction of T_0
dx_t: Axial deformation of the PC-bar after the introduction of T_0
dx_p: Embedding deformation of the anchorage plate after the introduction of T_0
dx_w: Compressive deformation of middle zone in CLT after the introduction of T_0
x_{g0}: Embedding deformation of column base after the introduction of T_0
x_t: Axial deformation at PC bar
x_{t0}: x_t after the introduction of T_0
K_t: Axial stiffness of PC bar
A_t: Cross-section area of PC bar
E_t: Elastic modulus of PC bar
h_t: PC bar length
x_p: Embedding deformation at the anchorage plate
x_{p0}: x_p after the introduction of T_0
x_w: Compressive deformation at middle zone in CLT
x_{w0}: x_w after the introduction of T_0

https://doi.org/10.52202/069179-0044

partial compression experiment described in Section 3.3. K_t, the stiffness of the PC bar is the axial stiffness, as shown in Eq. (14).

Figure 18 shows the stress distribution of the column base. For evaluating the column base, two simultaneous equations were solved, and the state of the compressive force was applied according to the degree of deformation. There are five stress distributions of the compressive force: (a) initial point, (b) anchor process, (c) limit anchor point, (d) elastic process, and (e) yield process. (a) The initial point is the state before horizontal deformation when the initial tension T_0 is applied. (b) The anchor process is a state in which the entire cross-section of the column base is in contact with the foundation, although horizontal deformation has occurred. (c) The limit anchor point is the state in which the entire cross-section is in contact, and the edge of the column base has no stress. (d) The elastic process is a state in which the stress distribution is triangular while the column base is uplifted. (e) The yield process is the state in which part of the stress distribution reaches the yield stress when the column base is uplifted.

In (a) Initial point, because horizontal deformation does not occur, there is no need to solve simultaneous equations for θ_{cb} and x_{n_cb}. So that, dT=0 and T_{cb}=T_0 from Eq. (7) and u_{cb}= − x_{g0} from Eq. (8).

Next, (b) anchor process must be evaluated, but this is not performed because it is very difficult to formulate. Therefore, because the deformation is small, (b) the anchor process is assumed to be in the elastic range and a skeletal curve is created by connecting (a) the initial point and (c) the limit anchor point with a straight line.

Next, (c) limit anchor point is presented. As the embedded width x_{n_cb}=w_c, the compressive force equation is given by Eq. (15), and the deformation compatibility equation is expressed by Eq. (16). These two equations were solved.

In (d), elastic process, the solutions of θ_{cb} and x_{n_cb} were obtained from the simultaneous equations of the compressive force C_{cb} (Eq. (17)) and compatibility equation (Eq. (18)).

In (e) yield process, Eq. (19) was used instead of Eq. (17). σ_{gy}, yield stress, and k_g, embedded stiffness, were used as the average yield stress and slope of the envelope obtained in the CLT-embedded experiment in Section 3.1. M_{cb} was calculated using Eq. (20).

The story deformation angle θ of the wall column is the sum of θ_{cb}: the column base rotation angle, θ_b, the storey deformation angle contribution of bending deformation, and θ_s, the storey deformation angle contribution of shear deformation, as shown in Eq. (22). Next, we demonstrate the effect of the stiffness involved in the series u_{cb} spring model on θ_{cb}. Figure 19 shows the deformation of the column base with a focus on θ_{cb}. As shown in Eq. (25), θ_{cb} can be calculated from u_{cb} and x_{ge}. x_{ge} means embedding deformation at the edge of the column base. u_{cb} is the sum of dx_t, dx_p, and dx_w with x_{g0} removed, as in Eq. (8). By rearranging Eq. (8), (22), and (25), Eq. (27) can be obtained. Therefore, θ_{cb} can be expressed as dx_t, dx_p, dx_w, and dx_g. Note that x_{ge} is the product of the rotation angle θ_{cb} and embedded width x_{n_cb} as shown in Eq. (26), and dx_g is the value obtained by subtracting x_{g0} from x_{we}, as shown in Eq. (28).

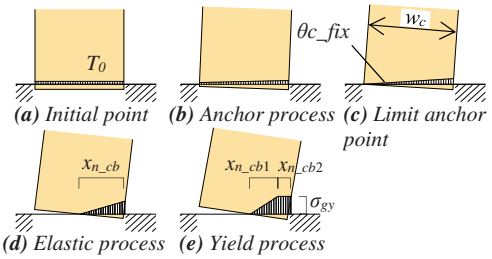

***Figure 18**: Stress distributions of the column base*

$$T_{cb\_fix} = C_{cb\_fix} = \frac{1}{2} k_g \theta_{cb\_fix} w_c^2 b \quad (15)$$

$$\theta_{cb\_fix} = \frac{-u_{cb}}{w_c / 2} \quad (16)$$

$$T_{cb} = C_{cb} = \frac{1}{2} k_g \theta_{cb} x_{n\_cb}^2 b \quad \{\text{same as Eq. (5)}\} \quad (17)$$

$$x_{n\_cb} = w_c / 2 - u_{cb} / \theta_{cb} \quad \{\text{same as Eq. (6)}\} \quad (18)$$

$$T_{cb} = C_{cb} = \frac{1}{2} k_g \theta_{cb} x_{n\_cb1}^2 b + \sigma_{gy} x_{n\_cb2} b \quad \{ x_{n\_cb} = x_{n\_cb1} + x_{n\_cb2} \} \quad (19)$$

$$M_{cb} = T_{cb} d_{cb} = T_{cb} (w_c / 2 - x_{n\_cb} / 3) \quad (20)$$

$$F = M_{cb} / h_f \quad (21)$$

$$\theta = \theta_{cb} + \theta_b + \theta_s \quad (22)$$

$$\theta_b = F h_f^2 / 3 E_w I_w \quad (23)$$

$$\theta_s = F / G_w A_w \quad (24)$$

T_{cb_fix}: Tension at Limit anchor point
C_{cb_fix}: Compressive force at Limit anchor point
θ_{cb_fix}: Rotation angle of column base at Limit anchor point
x_{n_cb1}: Embedded width of stiffness range
x_{n_cb2}: Embedded width of plastic range
σ_{gy}: Embedded yield stress of column base
h_f: Height of the point to apply force
θ_b: Story deformation angle contribution of CLT bending deformation
θ_s: Story deformation angle contribution of CLT shearing deformation
E_w: Elastic modulus of CLT
I_w: Cross-section secondary moment of CLT
G_w: Shear elastic modulus of CLT
A_w: Cross-section of CLT

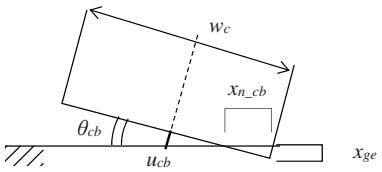

***Figure 19**: Deformation of column base focused on θ_{cb}*

$$\theta_{cb} = \frac{u_{cb} + x_{ge}}{w_c / 2} \quad (25)$$

$$x_{ge} = x_{n\_cb} * \theta_{cb} \quad (26)$$

$$\theta = \frac{2}{w_c} (dx_t + dx_p + dx_w + dx_g) + \theta_b + \theta_s \quad (27)$$

$$dx_g = x_{ge} - x_{g0} \quad (28)$$

x_{ge} : Embedding deformation at the edge of the column base
dx_g : Embedding deformation after the introduction of T_0

https://doi.org/10.52202/069179-0044

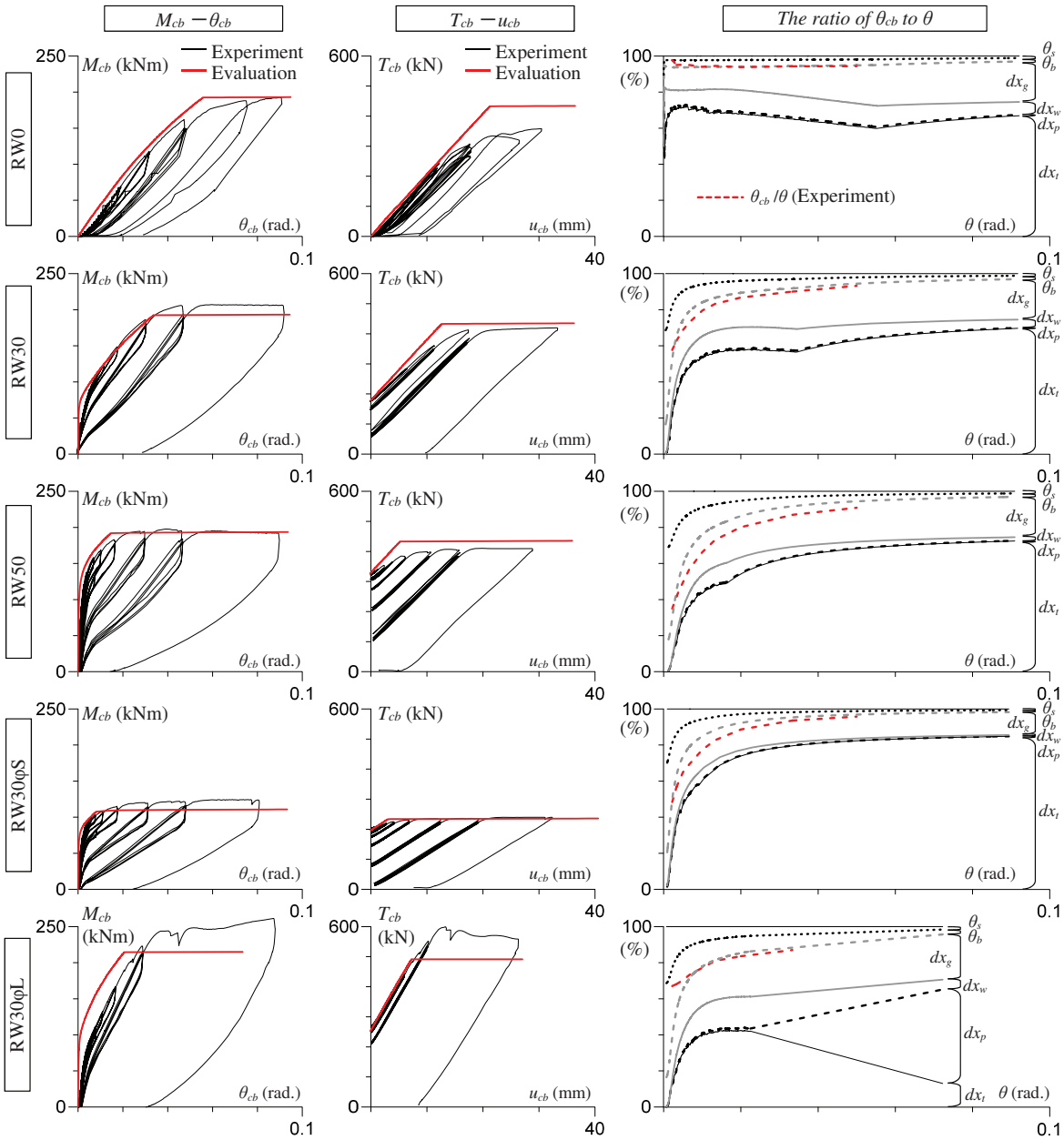

***Figure 20**: Compare the experiment and evaluation*

3.5 COMPARISON BETWEEN THE EXPERIMENT AND EVALUATION

Figure 20 compares the experimental and evaluation values. In the T_{cb}-u_{cb} relationship, the stiffness of RW30 and RW50 is slightly higher than the experimental value, but the evaluated value roughly reproduce the stiffness of the five experimental values. The yield points of RW0, 30, and 50 do not match, but the cause has not been elucidated. For RW30φL, in the experiments conducted to create the spring model in Chapters 3.2 and 3.3, the environment and equipment for applying a load of 500 kN or more could not be prepared. Therefore, deformation after reaching 500kN was not used as a reference.

In the M_{cb}-θ_{cb} relationship, the initial stiffness of RW30 and RW30φL were highly evaluated, but the other specimens reproduced the envelope of the experimental values well. Because T_g-δ_g relationship has a gentle slope when the stress is small, as shown in Figure 13, the experimental values of RW30 and RW30φL show lower initial stiffness than the evaluation values. Because the evaluation value does not reflect the part with low stiffness in the spring model, the evaluation value overestimated the initial stiffness. This aspect needs a more detailed examination in the future.

In θ_{cb}/θ, the horizontal axis is θ and the vertical axis is on the right side of Eq. (27). The distance between the lines corresponds to the proportion of the deformation that occupies θ. The dashed red line represents the experimental value of θ_{cb}/θ, which is compared with the sum of the ratios dx_t, dx_p, dx_w, and dx_g. In other words, the

https://doi.org/10.52202/069179-0044

dashed red line is compared with the dashed gray line. At RW0, dx_t was dominant for θ. Because the experimental (the dashed red line) and evaluation values of θ_{cb}/θ (the dashed gray line) are almost the same, the evaluation value can reproduce the deformation sharing of the rocking wall column without the initial tension. For RW30 and RW50, the effect of dx_t was small at small deformations, and dx_g, θ_b, θ_s were more dominant than RW0. The dashed gray line is the line of close shape to the experimental values of θ_{cb}/θ. RW30φS was influenced more by dx_t than RW30, i.e., the dashed gray line is a curve close to the experimental value of θ_{cb}/θ. In RW30φL, the deformation of the anchorage plate dx_p is dominant. Notably, the deformation of 500 kN or more cannot be used as a reference in relation to T_{cb}-u_{cb}, but the yield load of the PC-bar is approximately 800 kN, and the yield load of the CLT is considered to be even higher. Therefore, yielding at the anchorage plate was considered deterministic. In the experiment (Fig. 8), we confirmed a large deformation of the anchorage plate.

4 CONCLUSIONS

In this study, a static horizontal loading experiment was conducted on CLT wall columns with an origin return characteristic, by introducing prestress, and the mechanical behaviour of the CLT wall columns was investigated. We also proposed a method to evaluate the relationship between the bending moment and rotation angle of the column base. These are summarised as follows:

[Static horizontal loading experiment with CLT rocking-wall columns]

・ We determined the difference in the origin return characteristics and damage of wall columns when the prestress introduced to wall columns and the diameter of the PC steel bar was changed.

[Theoretical evaluation method]

・The proposed evaluation method was characterised by a detailed classification of the stress distribution of the column base and a detailed model of the uplift of the column base.

・Although the evaluation value has issues such as overestimating the initial slope of the M_{cb}–θ_{cb} relationship, the experimental value of some experimental specimens can be roughly reproduced.

ACKNOWLEDGEMENT

This research was supported by the 2016-2019 Grant-in-Aid for Scientific Research, Young Scientists (A): "Development of damping technology and proposal of damping design method for wooden high-scale buildings" (Project number: 16H06107, Research representative: Kazuhiro Matsuda). We would also like to thank Mr. Tomohiro Morimoto of Meiken Kogyo Co., Ltd., for his advice. In the experiment, I received the cooperation of Mr. Chisato Inutsuka, Mr. Keiichiro Goto, Mr. Masaki Sugimori and Mr. Yuta Hisada, former students at Meijo University. Here, we express our gratitude to you.

REFERENCES

[1] Japan Housing and Wood Technology Center: [2016 Building design and construction manual using CLT] CLT wo mochiita kenchikubutu no sekkei sekou manyuaru 2016 (in Japanese).

[2] Shimura S., Tsuda C., Hatakeyama T., Suganumata N., Suzuki K., Okabe M., Nakagawa T., Araki Y. and Tsutimoto T.: Study on Seismic Performance of Building Structure with Cross Laminated Timber Part4 Loading Test on a Frame, Summary of Technical papers of Annual meeting of AIJ, pp.311-312, 2012.9 (In japanese)

[3] Murakami S., Tsuchimoto T., Miura S., Isoda H., Miyake T., Yasumura M.: Study on Seismic Performance of Building Construction with Cross Laminated Timber No. 18 Plane test for large-size-panel of CLT, Summary of Technical papers of Annual meeting of AIJ, pp.569-570,2013.8 (In japanese)

[4] Matsuda, K., Kakuda, Y. and Sakata H.: Experimental Study on Mechanical Behavior of Passively Controlled Timber Structure with Self-Centering-Type CLT Wall Columns, WCTE, Coxe, Seoul, Republic of Korea, 2018.8

[5] Shiling Pei, John W. van de Lindt, Andre R. Barbosa, Jeffrey W. Berman, Eric McDonnell, J. Daniel Dolan, Hans-Erik Blomgren, Reid B. Zimmerman, Da Huang and Sarah Wichman : Experimental Seismic Response of a Resilient 2-Story Mass-Timber Building with Post-Tensioned Rocking Walls, 2019 American Society of Civil Engineers. (2019 ASCE), 2019.9

[6] Francesco Sarti, Allessandro Palermo, Stefano Pampanin: Development and Testin of an Alternative Dissipative Post-tensioned Rocking Timber Wall with Boundary Columns, ASCE Journal of Structural Engineering, E4015011, 2015.8

[7] Asif Iqbal, Stefano Pampanin, Massimo Fragiacomo, Alessandro Palermo, Andrew Buchanan: Seismic Response of Post-Tensioned LVL Walls Coupled with Plywood Sheets, World Conference on Timber Engineering,pp.291-296, 2012.7

[8] Horie Y., Isoda H., Matsuda M. Mori T., Tsuji T., Nakashima S. Araki Y. and Nakagawa T.: Full Scale Shaking Table Test of Structure Using CLT Rocking Shear Walls and Experimental Study of its Seismic Performance. Part 1: Structural System Overview and Pre-Analysis, Summary of Technical papers of Annual meeting of AIJ, pp.497-498,2022.9 (In japanese)

[9] Harada K., Koshihara M.,Araki Y., Tanaka K., Suzuki K, Hayasaki Y, Komoriya M.: Horizontal Loading test of high proof strength earthquake resisting walls using CLT panel(part1: Outline of the test and test models), Summary of Technical papers of Annual meeting of AIJ, pp.188-189, 2016. 8. (In japanese)

[10] Komoriya M., Hayasaki Y., Suzuki K., Harada K., Tanaka K., Araki Y., Koshihara M.: Horizontal Loading Test of High Proof Strength Earthquake Resisting Walls Using CLT Panel（Part2: The In-Plane Shear Test of Earthquake-Resisting Walls Using CLT Panel）, Summary of Technical papers

https://doi.org/10.52202/069179-0044

of Annual meeting of AIJ, pp.189- 190, 2016.8. (In japanese)
[11] Tanaka K., Harada K., Suzuki K., Hayasaki Y., Komoriya M., Araki Y. and Koshihara M.: Horizontal Loading Test of High Proof Strength Earthquake Resisting Walls Using CLT Panel （Part3: Estimation of the Structural Behavior by Elastic-plastic Analysis）, Summary of Technical papers of Annual meeting of AIJ, pp.191-192, 2016.8. (In japanese)
[12] Nagashima T., Tachibana K., Yano M. and Ohashi Y.: DESIGN METHOD FOR POST-TENSIONED TIMBER SHEAR WALL (PART 1): TRIANGULAR EMBEDMENT STIFFNESS AND BEHAVIOR IN ELASTIC RANGE, J. Struct. Constr. Eng., AIJ, Vol.85, No.770, pp. 539-548, 2020.3 (in Japanese)
[13] Inayama M: Study on structural design method of timber semi-rigid column-base joint drawn with tensile bolts, Summary of Technical papers of Annual meeting of AIJ, pp.624-622, Hokkaidou, 2013.8 (In japanese)

https://doi.org/10.52202/069179-0044